SMAR 2015 – Third Conference on Smart Monitoring,
Assessment and Rehabilitation of Civil Structures

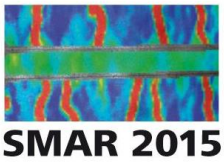


# Experimental testing and constitutive modeling of shape memory alloy confined concrete

Qiwen Chen and Bassem Andrawes

Department of Civil and Environmental Engineering, University of Illinois at Urbana-Champaign, Urbana, Illinois, USA.

ABSTRACT: Concrete confinement is an effective method to improve concrete strength and ductility. In recent years, a novel active confinement technique using shape memory alloys (SMAs) was proposed and proved to be promising to retrofit concrete structures with the aim of improving their seismic performance. Series of SMA confined concrete cylinders with different concrete strengths and spiral spacing were tested in order to understand the behavior of SMA confined concrete. Due to the unique feature of SMA confined concrete with a combination of active and passive confinement, no existing concrete constitutive model is able to capture its stress-strain behavior. Therefore, the authors propose a novel SMA confined concrete constitutive model based on the Drucker-Prager plasticity model to predict and simulate the stress-strain behavior of SMA confined concrete.

## 1 INTRODUCTION

Concrete confinement has been widely studied by researchers and it was shown that concrete confinement can significantly improve the strength and ductility of concrete (Richart *et al.* 1928; Sheikh *et al.* 1982; Scott *et al.* 1982; Mander *et al.* 1988; Mirmiran and Shahawy 1997). There are mainly two types of concrete confinement, passive and active. Internal transverse steel reinforcement, external steel jackets, fiber reinforced polymer (FRP) jackets are commonly used as passive confinement approaches, in which, passive confining pressure develops as concrete dilates during loading. On the other hand, active confining pressure is applied to concrete prior to loading. Previous researchers have proved that active confinement is more effective than passive confinement in improving concrete strength and ductility. In order to make use of the effectiveness of active confinement, some researchers proposed to apply active confining pressure to concrete structures (Fam and Rizkalla 2001; Nesheli and Meguro 2006; Moghaddam *et al.* 2010) using prestressing tendons, prestressed steel jackets or prestressed FRP straps, etc. However, due to the extensive cost, labor and special hardware required, the application of active confinement in practice is still limited. Recently, Andrawes and Shin (2008) proposed the idea of using SMA spirals to confine RC columns to improve their ductility. Later, Shin and Andrawes (2010) conducted compressive tests on SMA confined concrete cylinders and compared the behavior with those from FRP confined cylinders. Shin and Andrawes (2011) applied the SMA confinement technique to retrofit RC columns and compared their behaviors with that of columns retrofitted by FRP jackets. Chen *et al.* (2014) investigated applying SMA confinement to non-circular concrete columns and proved its superior in improving the ductility of square concrete

elements compared to FRP confinement. SMA is a type of alloys that are able to recover its original shape through phase transformation. In the SMA confinement technique, SMA wires are first prestrained in their martensite phase, then wrapped around concrete columns and heated above a certain temperature using propane torch in order to activate shape memory effect. The constraint from concrete limits the SMA from recovering their original shape and hence recovery stress develops along the wires, which in turn applies active confinement to the concrete. The behavior of SMA confined concrete is different from pure actively and passively confined concrete, since it is a combination of active and passive confinement, because constant active confinement in the SMA confined concrete is applied to the concrete prior to loading through SMA heating and passive confinement keeps increasing as concrete dilates during loading. However, few experimental studies of this novel SMA confinement technique have been conducted and more in depth investigations are in great need to better understand the unique behavior of SMA confined concrete. Besides, no existing concrete constitutive model is able to capture its stress-strain behavior. Hence, this paper proposes a novel SMA confined concrete constitutive model to simulate the stress-strain behavior of SMA confined concrete.

## 2 EXPERIMENTAL INVESTIGATION

A total of 13 concrete cylinders with a diameter of 152.4 mm and a height of 305 mm were prepared and tested in this experimental study. Table 1 displays the characteristics of all tested specimens, including unconfined concrete strength, spirals spacing and design active confining pressure, as well as test results summary which will be discussed later in the paper. Active confining pressures shown in Table 1 were calculated based on the methods proposed by Mander *et al.* (1988) and were computed according to the corresponding SMA wires recovery stress (607 MPa). Prior to compressive loading, SMA spirals were heated to activate the shape memory effect using propane torch. All the specimens were loaded using a 600-kip hydraulic load frame with a loading/unloading strain rate of 0.5%/min and using displacement control.

Table 1. Test specimens and result summary of cyclically loaded SMA confined concrete

| Label | Concrete Strength (MPa) | Spiral Pitch (mm) | Active Confinement (MPa) | Peak Stress (MPa) | Peak Strain | Ultimate Stress (MPa) | Ultimate Strain | Residual Stress @ 2.5% Axial Strain (MPa) |
|---|---|---|---|---|---|---|---|---|
| UC-B1C | 30.5 | - | 0 | 30.5 | 0.0016 | - | - | - |
| SMA-B1S2C | | 15.9 | 1.22 | 44.9 | 0.0027 | 16.9 | 0.0663 | 20.4 |
| SMA-B1S3C | | 10.2 | 1.94 | 40.4 | 0.0035 | 30.9 | 0.1005 | 28.1 |
| SMA-B1S4C | | 5.1 | 3.95 | 56.9 | 0.0057 | 46 | 0.053 | 47.1 |
| UC-B2C | 39.6 | - | 0 | 39.6 | 0.0022 | - | - | - |
| SMA-B2S1C | | 25.4 | 0.91 | 45.1 | 0.0027 | 14.4 | 0.0533 | 17.4 |
| SMA-B2S2C | | 19.1 | 1.24 | 46.0 | 0.0032 | 19 | 0.0523 | 19.7 |
| SMA-B2S3C | | 12.7 | 1.9 | 49.3 | 0.0038 | 24 | 0.0765 | 28.9 |
| SMA-B2S4C | | 6.4 | 3.88 | 59.8 | 0.0070 | 48.9 | 0.1198 | 45.6 |
| UC-B3C | 50.0 | - | 0 | 49.9 | 0.0022 | - | - | - |
| SMA-B3S2C | | 19.1 | 1.24 | 58.1 | 0.0031 | 18.9 | 0.0585 | 19.7 |
| SMA-B3S3C | | 12.7 | 1.9 | 64.2 | 0.0037 | 27.7 | 0.0958 | 28 |
| SMA-B3S4C | | 6.4 | 3.88 | 80.6 | 0.0056 | 44.8 | 0.0641 | 42.6 |

As indicated in Table 1, for SMA confined concrete specimens with concrete strength of 39.6 MPa, the peak stresses of concrete with spiral spacing 25.4 mm, 19.1 mm, 12.7 mm, and 6.4 mm

increased by 13.9%, 16.2%, 24.6%, and 51.1%, respectively compared to that of the unconfined concrete strength. The ultimate strains were 0.0533 mm/mm, 0.0523 mm/mm, 0.0765 mm/mm and 0.1198 mm/mm, respectively and the corresponding ultimate stresses were 32.0%, 41.3%, 48.6% and 81.8% of the peak stresses. Similar results were observed for cases with different concrete strength and therefore it can be concluded that the effectiveness of SMA confinement on strength and ductility enhancement increases as the SMA spiral spacing decreases. Comparing SMA-B2S1C (active confinement: 0.91 MPa) and SMA-B2S2C (active confinement: 1.24 MPa), the differences in both peak stress and ultimate strain were only 2%. Therefore, it was assumed that the lower bound of active confinement for using SMA confinement effeciently is 1.24 MPa. Fig. 1 compares the failure modes of SMA-B2S1C, SMA-B2S2C, SMA-B2S3C, and SMA-B2S4C. All the specimens confined with SMA spirals showed a clear diagonal shear cracks and failed due to the rupture of SMA. Concrete confined by SMA spirals with smaller spacing encountered more local crushing before the rupture of the SMA spirals (failure); while with larger spacing, lateral deformation developed faster in the early stage and the specimen failed due to the large shear crack opening without too much local crushing and damage. Fig. 2 compares the envelopes of the axial stress-strain curves from cyclically loaded SMA confined concrete specimens with different concrete strength, but with the same level of active confining pressure. Fig. 2(a) compares the specimens with active confining pressure of 1.2 MPa. As the specimens were loaded beyond the peak stress, all three specimens with varied concrete strength decreased to a similar level of residual stresses at about 2.5% axial strain, 20.4 MPa, 19.7 Mpa and 19.7 MPa, respectively, and approximately maintained a plateau until reaching the ultimate strain. Similar phenomenon was also observed for the cases with active confining pressure of 1.9 MPa and 3.9 MPa. Therefore, regardless of concrete strength, active confining pressure is the dominant factor that determines the stress plateau of SMA confined concrete.

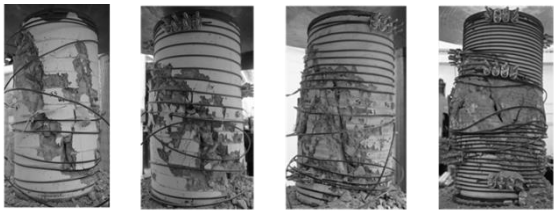


Figure 1. Failure mode of SMA confined concrete

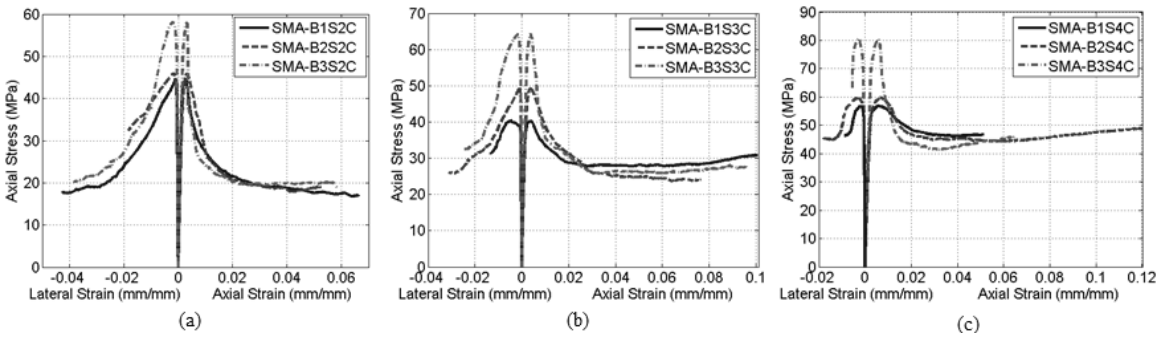


Figure 2: SMA confined concrete stress-strain behavior with the same active confinement and varied concrete strength

## 3 CONSTITUTIVE MODEL

Despite the experimental work done on SMA confinement technique over the last few years, the numerical efforts are still lacking. Due to the unique feature of SMA confined concrete, a combination of active and passive confinement, stress-strain models that exist in the literature are incapable of predicting and modeling the behavior of SMA confined concrete. Existing concrete models can be mainly divided into two types. One type is based on empirical equations to fit the stress-strain relationship obtained from experimental testing; while the other is based on the theory of plasticity to describe the three-dimensional constitutive relationship of concrete. Since empirical equations are usually represented using one-dimensional stress-strain relation and assume constant confining pressure, they are unable to describe the triaxial stress-strain behavior of SMA confined concrete due to varying confining pressure during loading. Therefore, with the aim of modeling the unique three-dimensional behavior of SMA confined concrete, plasticity approach was utilized in this paper. Plasticity models are characterized by three important components, namely, yield criterion, hardening/softening function and flow rule. Yield criterion describes yield surfaces by using stress invariants. When the material first reaches the yield surface, plastic deformation is initiated. Hardening/softening of material determines the subsequent yield surfaces after first yield. Flow rule determines the direction and magnitude of plastic deformation. Previous research has been done on using plasticity model to simulate the three-dimensional behavior of confined concrete (Lubliner *et al.* 1989; Oh 2002; Yu *et al.* 2010) and proved that plasticity model is able to simulate the three-dimensional behavior of confined concrete. Therefore, a concrete plasticity model was calibrated based on Drucker-Prager model. Note that, unless specify, compression is negative and tension is positive in this paper. Drucker-Prager yield function utilized in this paper is shown in Eq. 1.

$$\sqrt{J_2} + \theta I_1 - k = 0 \tag{1}$$

where, $J_2$ and $I_1$ are second deviatoric stress invariant and first stress invariant, respectively; $k$ is the hardening/softening function; $\theta$ is frictional angle and its calculation was described in Chen (1982), Oh (2002) and Yu *et al.* (2010). This frictional angle is a material property that can be derived from experimental results. This parameter was equal to 0.2934 based on Richart *et al.* (1928) for actively confined concrete and was equal to 0.2634 based on Teng *et al.* (2007) for FRP confined concrete. According to the relationship between Mohr-Coulomb yield surface and Druker-Prager yield surface, the frictional angle for SMA confined concrete is 0.3503.

Hardening/softening function $k$ represents the first and subsequent yield surface and it is related to the plastic work is done. It has been proved that hardening/softening function of confined concrete is determined by concrete strength, lateral confinement and plastic deformation (Oh 2002; Yu *et al.* 2010; Chen *et al.* 2014). Based on the hardening/softening function from experimental results, Eq. 2 was adopted to describe the hardening/softening function at the range before it reaches the plateau. After reaching the residual value $k_{resi}$, the hardening/softening values are assumed to be constant $k_{resi}$ for simplicity.

$$Y = \frac{mX}{1 + \left(m - \dfrac{n}{n-1}\right)X + \dfrac{X^n}{n-1}} \tag{2}$$

where $Y = k / k_{peak}$ ; $X = \hat{\varepsilon}^p / \hat{\varepsilon}^p_{k,peak}$ ; $\hat{\varepsilon}^p$ is the equivalent plastic strain and $\hat{\varepsilon}^p_{k,peak}$ is the equivalent plastic strain at the peak of hardening/softening function, and incremental equivalent plastic strain is defined as $\Delta\hat{\varepsilon}^p = \sqrt{\Delta\varepsilon_c^p + \Delta\varepsilon_l^p + \Delta\varepsilon_l^p}$ ; $m = \partial Y / \partial X = E_0^k / E_p^k$, which controls

the ascending slope, and $E_0^k$ is the initial slope of the hardening/softening function $E_p^k = k_{peak} / \hat{\varepsilon}_{k,peak}^p$; $n$ is a parameter controls the descending slope. Parameters $E_0^k$, $k_0$, $k_{peak}$, $\hat{\varepsilon}_{k,peak}^p$, $k_{resi}$, and $n$ were calibrated using experimental data and they can be calculated using Eq. 3-8, where $f_{l,a}$ is the active confining pressure, $f_{co}^{'}$ is the unconfined concrete strength and $\varepsilon_{co}$ is the axial strain coresponding to the peak stress of unconfined concrete.

$$E_0^k = -270433 f_{l,active} / f_{co}^{'} + 45972 \ (MPa) \ \ \left(R^2 = 0.834\right) \tag{3}$$

$$k_0 = \left(-0.6958 f_{l,active} / f_{co}^{'} + 0.1071\right) \cdot \left(-f_{co}^{'}\right) \ (MPa) \ \ \left(R^2 = 0.824\right) \tag{4}$$

$$k_{peak} = 0.266\left(-f_{co}^{'}\right)(MPa) - 1.421 \ \ \left(R^2 = 0.876\right) \tag{5}$$

$$\hat{\varepsilon}_{peak}^p = \left(7.461 f_{l,active} / f_{co}^{'} + 1.036\right) \cdot \left(-\varepsilon_{co}\right) \ \ \left(R^2 = 0.795\right) \tag{6}$$

$$k_{res} = 0.7255\left(-f_{l,active}\right)(MPa) + 1.077 \ \ \left(R^2 = 0.913\right) \tag{7}$$

$$n = 0.0144\left(-f_{co}^{'}\right)(MPa) + 1.582 \ \ \left(R^2 = 0.795\right) \tag{8}$$

Flow rule features the plastic deformation direction. A non-associated flow rule was utilized in the proposed model, which was realted to concrete strength, plastic deformation and lateral confining pressure (Oh 2002; Yu *et al.* 2010). The Drucker-Prager type potential function $G$ was adopted (Eq. 9) in the proposed model.

$$G = \sqrt{J_2} + \psi I_1 \tag{9}$$

where, $\psi$ is potential function parameter to be determined based on the deformation characteristics. To describe the potential flow for confined concrete, dilation rate $\alpha$ was used and it can be calculated based on axial stress-strain relation, axial-lateral strain relation, and Eq. 10 (Oh 2002; Yu *et al.* 2010).\

$$\alpha = \sqrt{3}\frac{\Delta\varepsilon_c^p + 2\Delta\varepsilon_l^p}{\left|\Delta\varepsilon_c^p - \Delta\varepsilon_l^p\right|} = \sqrt{3}\frac{1 + 2\Delta\varepsilon_l^p / \Delta\varepsilon_c^p}{\Delta\varepsilon_l^p / \Delta\varepsilon_c^p - 1} = 6\psi \tag{10}$$

where $\Delta\varepsilon_c^p$ is incremental axial plastic strain; $\Delta\varepsilon_l^p$ is incremental lateral plastic strain. According to the test results, dilation rate function increases from the initial value $\alpha_0$, and after it reaches a peak value $\alpha_{peak}$, it decreases to a plateau $\alpha_{resi}$. To represent these features, Eq. 2 was still suitable and was chosen to describe the dilation rate function at the range before it reaches the plateau. After reaching the residual value $\alpha_{resi}$, the dilation rate is assumed to be constant $\alpha_{resi}$ for simplicity. However, using Eq. 2 for the dilation rate model, the definition of $X$, $Y$, $m$ and $n$ were different. $Y = \left(\alpha - \alpha_0\right) / \left(\alpha_{peak} - \alpha_0\right)$; $X = \hat{\varepsilon}^p / \hat{\varepsilon}_{\alpha,peak}^p$; $\hat{\varepsilon}_{\alpha,peak}^p$ is the equivalent plastic strain at the peak of dilation rate function; $m = E_0^\alpha / E_p^\alpha$, which controls the ascending slope, and

$E_0^{\alpha}$ is the initial slope of the dilation rate function, $E_p^{\alpha} = \left(\alpha_{peak} - \alpha_0\right) / \hat{\varepsilon}_{\alpha,peak}^{p}$. The initial dilation rate $\alpha_0$ can be determined using Eq. 10 by substituting Poisson's ratio (dilation rate in the elastic range) $\nu = -\Delta\varepsilon_l^p / \Delta\varepsilon_c^p$. Assuming $\nu = 0.18$, one can obtain $\alpha_0 = -0.9394$. Parameters $E_0^{\alpha}$, $\alpha_{peak}$, $\hat{\varepsilon}_{\alpha,peak}^{p}$, $\alpha_{resi}$, and $n$ were calibrated using experimental data and they can be calculated using Eq. 11-15.

$$E_0^{\alpha} = \begin{cases} -11722\, f_{l,active} / f_{co}^{'} + 1417.3\ (MPa) & \left(f_{l,active} / f_{co}^{'} \le 0.1\right) \\ 245.1\ (MPa) & \left(f_{l,active} / f_{co}^{'} > 0.1\right) \end{cases} \quad \left(R^2 = 0.770\right) \tag{11}$$

$$\alpha_{peak} = \frac{0.1357}{\left(f_{l,active} / f_{co}^{'} + 0.0261\right)} \quad \left(R^2 = 0.980\right) \tag{12}$$

$$\hat{\varepsilon}_{\alpha,peak}^{p} = \frac{\left(-\varepsilon_{co}\right)\left(3.708\, f_{l,active} / f_{co}^{'} + 0.0212\right)}{\left(f_{l,active} / f_{co}^{'} - 0.0118\right)} \quad \left(R^2 = 0.948\right) \tag{13}$$

$$\alpha_{res} = -16.468\, f_{l,active} / f_{co}^{'} + 1.176 \quad \left(R^2 = 0.993\right) \tag{14}$$

$$n = \begin{cases} -111.6\, f_{l,a} / f_{co}^{'} + 8.464 & \left(f_{l,a} / f_{co}^{'} < 0.04\right) \\ 4 & \left(f_{l,a} / f_{co}^{'} \ge 0.04\right) \end{cases} \quad \left(R^2 = 0.961\right) \tag{15}$$

In order to reflect the unloading and reloading stiffness degradation of SMA confined concrete during cyclic loading, it is important to define a damage parameter. In the proposed model, the following assumption is made for simplicity: (1) unloading and reloading stiffness is the same; (2) stress and strain are linear related between unloading point and reloading point. Damage parameter is defined as $d = 1 - E_r / E_c$, where $E_r$ is the reloading modulus of SMA confined concrete at a certain axial strain and $E_c$ is the elastic modulus of the concrete. Eq. 16 was chosen to model the damage parameter and the two undetermined parameters $a$ and $b$ can be calibrated based on experimental results.

$$d = 1 - \frac{E_r}{E_c} = -a \ln\left(\varepsilon_c\right) + \left(1 - b\right) \tag{16}$$

$$a = 0.0085\, f_{l,a} - 0.1717 \quad \left(R^2 = 1.0\right) \tag{17}$$

$$b = -a \ln\left(0.1764\, f_{l,a} + 0.0082\right) \quad \left(R^2 = 1.0\right) \tag{18}$$

Figure 3 compares the experimental results and proposed model for both the axial stress-axial strain and axial stress-lateral strain relation under cyclic loading. One can find that the proposed plasticity model was able to predict the stress-strain relation of SMA confined concrete with very good accuracy. Table 2 shows the ratio between model predicted results and experiment result for peak axial stress, and its corresponding axial strain, ultimate stress and ultimate strain, as well as the axial stress at 2.5% axial strain. The error of stress prediction is far less than strain and the

average prediction to experiment ratios of peak stress, ultimate stress and axial stress at 2.5% are 0.998, 1.028, and 0.985, respectively, with standard deviation less than 6.5%.

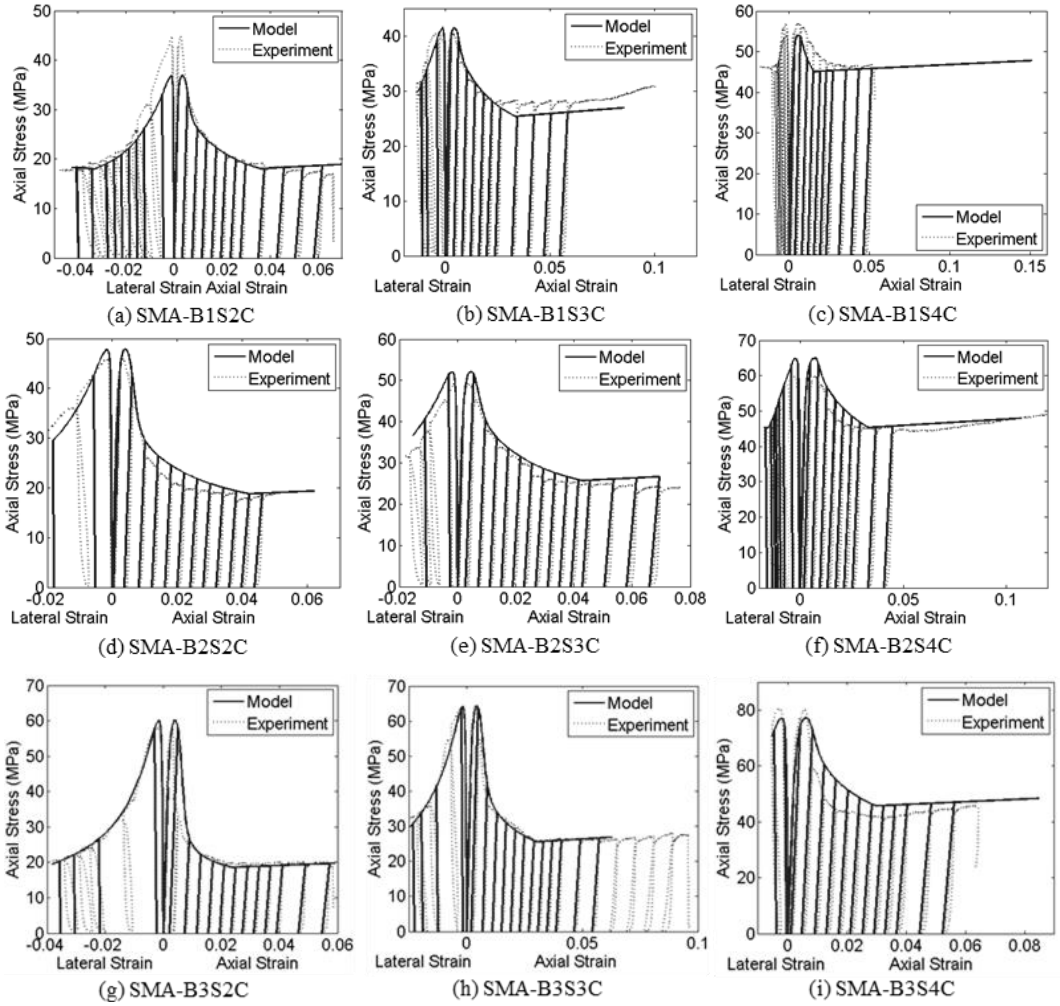


Figure 3. Comparison of axial stress-axial strain and axial stress-lateral strain from experimental results and with the proposed model

Table 2. Ratio between plasticity model predicted values and experimental results

| | Strength (MPa) | Pitch (mm) | Peak Stress | Peak Strain | Ultimate Stress | Ultimate Strain | Axial Stress @ 2.5% |
|---|---|---|---|---|---|---|---|
| SMA-B1S2C | | 15.9 | 0.823 | 1.278 | 1.118 | 1.048 | 0.929 |
| SMA-B1S3C | 30.6 | 10.2 | 1.024 | 1.157 | 0.872 | 0.852 | 0.957 |
| SMA-B1S4C | | 5.1 | 0.949 | 1.014 | 1.038 | 2.840 | 1.015 |
| SMA-B2S2C | | 19.1 | 1.042 | 1.255 | 1.021 | 1.190 | 0.985 |
| SMA-B2S3C | 39.6 | 12.7 | 1.057 | 1.205 | 1.112 | 0.910 | 0.921 |
| SMA-B2S4C | | 6.4 | 1.086 | 1.036 | 0.980 | 0.895 | 1.051 |
| SMA-B3S2C | | 19.1 | 1.035 | 1.308 | 1.042 | 1.009 | 0.999 |
| SMA-B3S3C | 50.0 | 12.7 | 1.001 | 1.182 | 0.971 | 0.655 | 0.958 |
| SMA-B3S4C | | 6.4 | 0.956 | 1.073 | 1.080 | 1.322 | 1.136 |
| Average | | | 0.998 | 1.620 | 1.028 | 1.126 | 0.985 |
| Standard Deviation | | | 0.065 | 1.560 | 0.065 | 0.518 | 0.063 |

## 4 CONCLUSIONS

This study first focused on experimentally investigating the behavior of SMA confined concrete. Cyclic compressive tests were conducted on 13 cylinders confined with four different spiral spacing (active confining pressure ranging from 0.91-3.95 MPa) and with three different levels of concrete strength ranging from 30.6 MPa to 50.0 MPa. Then, a concrete plasticity model was calibrated within the framework of Drucker-Prager model to predict and simulate the unique behavior of SMA confined concrete. Based on the experimental results and the proposed consititutive model, the the following conclusions can be drawn:

- The effectiveness of SMA confinement on strength and ductility enhancement increases as the SMA spiral spacing decreases;
- Regardless of concrete strength, active confining pressure is the dominant factor that determines the stress plateau (residual stress) of SMA confined concrete;
- The proposed model is able to capture the stress-strain behavior of SMA confined concrete accurately including peak stress (0.2% error on average), axial stress at 2.5% strain (1.5% error on average), ultimate stress (2.8% error on average), ultimate strain (4.7% error on average, excluding two outliners), as well as the stiffness degradation during cyclic loading.

## AKNOWLEDGMENT

The authors acknowledge the financial support provided for this research by the National Science Foundation through its Faculty Early Career Development (CAREER) program under Award No. 1055640.

## REFERENCES

Andrawes, B., and Shin, M. 2008. Seismic retrofitting of bridge columns using shape memory alloys. *Proceedings of SPIE - The International Society for Optical Engineering*, 6928.

Chen, Q., and Andrawes, B. 2014. Finite element analysis of actively confined concrete using shape memory alloys. *J. Advanced Concrete Tech*. 12: 520-534.

Chen, Q., Shin, M., and Andrawes, B. 2014. Experimental study of non-circular concrete elements actively confined with shape memory alloy wires. *Constr. Build. Mater*., 61: 303-311.

Chen, W. F. 1982. Plasticity in reinforced concrete. McGraw-Hill Book Company.

Fam, A.Z., and Rizkalla, S.H. 2001. Confinement model for axially loaded concrete confined by circular fiber-reinforced polymer tubes. *ACI Struct. J.*, 98(4): 451-461.

Lubliner, J., Oliver, J., Oller, S., and Onate, E. 1989. A plastic-damage model for concrete. *Int. J. Solid Struct.*, 25:299-329.

Mander, J.B., Priestley, M.J.N., and Park, R. 1988. Theoretical stress-strain model for confined concrete. *J. Struct. Eng.*, 114(8): 1804–1826.

Mirmiran, A., and Shahawy, M. 1997. Behavior of concrete columns confined by fiber composites. *J. Struct. Eng.*, 123(5): 583-590.

Moghaddam, H., Samadi, M., Pilakoutas, K., and Mohebbi S. 2010. Axial compressive behavior of concrete actively confined by metal strips, part A: experimental study. *Mater. Struct.*, 43(10): 1369-1381.

Nesheli, K.N., and Meguro, K. 2006. Seismic retrofitting of earthquake-damaged concrete columns by lateral pre-tensioning of FRP belts. *Proceedings of the Eighth U.S. National Conference on Earthquake Engineering 2006, Paper No. 841*. San Francisco, U.S.

Oh, B. 2002. A plasticity model for confined concrete under uniaxial loading. Ph.D. thesis, Lehigh University.

Richart, F.E., Brandtzaeg, A., and Brown, R.L. 1928. A study of the failure of concrete under combined compressive stresses. *Rep. No. 185, Univ. of Illinois Engineering Station, Urbana, IL*.

Scott, B.D., Park, R., and Priestley, M.J.N. 1982. Stress-strain behavior of concrete confined by overlapping hoops at low and high strain rates. *ACI J.*, 79(1): 13-27.

Sheikh, S.A., and Uzumeri, S.M. 1982. Analytical model for concrete confinement in tied columns. *J. Struct.*, 108(12): 2703-2722.

Shin, M., and Andrawes, B. 2010. Experimental investigation of actively confined concrete using shape memory alloys. *J. Eng. Struct.*, 32(3): 656-664.

Shin, M., and Andrawes, B. 2011. Lateral cyclic behavior of reinforced concrete columns retrofitted with shape memory spirals and FRP wraps. *J. of Struct. Eng.*, 137(11): 1282-1290.

Teng, J.G., Huang, Y.L., Lam, L., and Ye, L.P. 2007. Theoretical model for fiber reinforced polymer-confined concrete. *J. Compos. Constr.*, 11(2): 201-210.

Yu, T., Teng, J.G., Wong, Y.L., and Dong, S.L. 2010. Finite element modeling of confined concrete-I: Drucker-Prager type plasticity model. *Eng. Struct.*, 32(3):665-679.